



HAL
open science

Advanced approach for static part of loss-surface iron loss model

O. Messal, A-T Vo, M. Fassenet, P. Mas, S. Buffat, A. Kedous-Lebouc

► **To cite this version:**

O. Messal, A-T Vo, M. Fassenet, P. Mas, S. Buffat, et al.. Advanced approach for static part of loss-surface iron loss model. *Journal of Magnetism and Magnetic Materials*, 2020, 24th Soft Magnetic Materials (SMM) Conference, 502, pp.166401. 10.1016/j.jmmm.2020.166401 . hal-03027309

HAL Id: hal-03027309

<https://hal.science/hal-03027309>

Submitted on 29 Nov 2020

HAL is a multi-disciplinary open access archive for the deposit and dissemination of scientific research documents, whether they are published or not. The documents may come from teaching and research institutions in France or abroad, or from public or private research centers.

L'archive ouverte pluridisciplinaire **HAL**, est destinée au dépôt et à la diffusion de documents scientifiques de niveau recherche, publiés ou non, émanant des établissements d'enseignement et de recherche français ou étrangers, des laboratoires publics ou privés.

Advanced Approach for Static Part of Loss-Surface Iron Loss Model

O. Messal^{1,2}, A-T Vo^{1,*}, M. Fassenet¹, P. Mas³, S. Buffat³, A. Kedous-Lebouc¹

¹ Univ. Grenoble Alpes, Grenoble INP, CNRS, G2Elab, F-38000 Grenoble – France

² Univ. Lille, Arts et Metiers ParisTech, Centrale Lille, HEI, EA 2697 - L2EP, F-59000 Lille, France

³ Schneider Electric, F-38320 Eybens – France

KEYWORDS

Static hysteresis, Loss Surface model, magnetic material modeling, hysteresis model, iron loss

ABSTRACT

Hysteresis models allow the prediction of iron losses in materials under complex magnetic excitation, with accuracy depending on their principle and identification procedure. Commonly, to achieve high accuracy, a model may require a broad set of experimental input data, which is in some cases, not easy to obtain. We propose, in this study, a static model focusing on simplicity while still striving for accuracy. Its principle is to represent the variation of the field deviation between reversal curves and a near saturation hysteresis loop. In terms of input data, this model requires the experimental first magnetization curve and a few quasi-static centered hysteresis loops of the material. Following the principle description, the identification procedure, the model validation, as well as a sensitivity study are presented in detail.

1. INTRODUCTION

Electrical machines are the dominant type of load in industry, so improving their efficiency can help to reduce overall energy consumption and so on climate change. For this reason, stricter international standards have been approved and imposed in the European Union, the United States, and other markets [1]. Machine efficiency can be enhanced through a thorough understanding of the problems associated with power losses, one of the most important being iron losses. Therefore, we should apply from the design phase accurate iron loss models. Given the widespread use of switched-mode power supplies, magnetic excitation becomes considerably more complicated, and conventional loss separation approaches [2]–[4] have inadequate performance. Better results can be obtained using empirical coefficients or approaches, as in [5]–[12], whose application is often limited. Another solution is to implement hysteresis models that have greater accuracy. These models can reconstruct the hysteresis loop of any excitation waveform and then deduce the iron loss by the enclosed area of this loop. Each model has its advantages, namely accuracy, identification complexity, implementation complexity, and calculation time. In this study, an exhaustive review of the existing models is not our concern; an overview and comparison can be found in [13].

The accuracy of a model [14]–[24] depends on assumptions taken into account to simplify what really happened physically, as well as the quantity and complexity of experimental data used for the identification stage. It appears that some models, particularly purely mathematical ones [15], [19], require larger and more complex set of data than the others. Given the fact that in most engineering research and development centers, magnetic data of materials such as specific hysteresis loops and reversal curves are not always available, the implementation capability of some models can be limited. For this reason, we have developed the Loss Surface model over the past twenty years to provide a simple but effective solution to predict iron losses [25]–[29]. The model is valid for any induction waveforms, even the most deformed ones generally found in electrical machines. It separates the hysteresis behavior of materials into static and dynamic parts. The dynamic behavior is identified by a single surface $S = H_{dyn}(B, dB/dt)$ and the static one can be described by any existing static model. Initially, we have used a similar Preisach model for this work [26]; however, it does not meet the simplicity criteria, and a new replacement is then proposed and presented in this paper. This static model is based on a few experimental data, such as the experimental first magnetization curve, essential for any FEM simulation, a high induction centered hysteresis loop, and a few centered-loops at lower levels. The first part of the paper is devoted to a detailed description of the theoretical basis to give an overview of different notions and concepts. Among them, the unit differential reversal curve (**uRDC**) is a completely new concept, which plays a prominent role in our modelling approach. Then, the reliability and robustness of the model are demonstrated by a sensitivity study and comparisons between simulation results and measurements performed on the standardized Epstein frame and ring specimens.

2. PRINCIPLE DESCRIPTION

* anh-tuan.vo@g2elab.grenoble-inp.fr

In [16], Jiles decomposed the total magnetization into two contributions, the reversible and the irreversible. The reversible component refers to the domain wall bending, which occurs depending on the domain wall surface energy, the strength of the pinning sites (intrinsic factors) and the difference between the prevailing magnetization and the anhysteretic magnetization at the same field (extrinsic factor). On the other hand, the irreversible part is explained by the pinning process during the domain wall displacement. This theory has been the subject of a broad consensus and also criticism [30] in successive studies, always on its physical basis. Despite its questionable physical explanation, and inadequate performance in the case of minor hysteresis loops, this model is extensively applied due to its relatively simple implementation. In this paper, the proposed model is also constructed on the basis of the decomposition principle, which is done on the total static magnetic field H_{stat} (1), contrary to Jiles' approach on the total magnetization M . The input of our model is the time variation of the bulk flux density B , the output is the static field H_{stat} , which is composed of two contributions, H_{anhys} and H_{comp} .

$$H_{stat} = H_{anhys} + H_{comp} \quad (1)$$

The contribution H_{anhys} represents the anhysteretic field (described by the thermodynamic equilibrium state), which requires prior knowledge of the anhysteretic curve. This curve, instead of being determined by the field cycling method or the thermal demagnetization [31], is approximately specified by the median curve (red curve in Fig. 1a) of a near saturation hysteresis loop or the major loop (black curve in Fig. 1a). In the case of our model, H_{anhys} is assumed to be history independent which means that at any magnetization state, it is deduced from a look-up table $H_{anhys} - B$, or through an arbitrary function, which fits experimental anhysteretic curve, such as the modified Langevin expression in Jiles' model [16]. The history dependence or the mechanism of memory formation of the magnetic hysteresis is exposed through the H_{comp} component (*comp* as complementary), which represents the magnetic field caused by both the bending and displacement of the domain wall. As a consequence, the main issue now is the modelling approach of H_{comp} . It can be described directly by a mathematic function or divided into components that can be described mathematically in a simpler way.

From (1), H_{comp} curve of any hysteresis loop can be obtained by subtracting the anhysteretic field H_{anhys} from the static field of the hysteresis loop. For instance, in Fig. 1a, there are two hysteresis loops, the major and an intermediate, the H_{comp} of these loops are represented in Fig. 1b respectively by the blue and the yellow curves. The blue one includes two symmetrical parts: a positive bound associated to the increasing B and a negative one associated to the decreasing B . It is particularly named H_{env} representing the complementary component of the major envelope. A particular transformation of (1) leads to a clearer definition of H_{env} in (2).

$$H_{env} = H_{stat}^{major} - H_{anhys} \quad (2)$$

Another worth noted quantity is ΔH , which is the difference between the static field of any hysteresis loop and the major envelope. We have:

$$\Delta H = H_{stat} - H_{stat}^{major} = (H_{stat} - H_{anhys}) - (H_{stat}^{major} - H_{anhys}) = H_{comp} - H_{env} \quad (3)$$

The quantities H_{comp} , H_{env} and ΔH are geometrically interpreted by colored arrows in Fig. 1. In fact, H_{comp} of the small hysteresis loop is difficult to be modelled because of its complex variation. However, as can be observed, the quantity $\Delta H(B)$ varies quite monotonously. It is canceled out gradually from the initial value ΔH_{rev} to the final value ΔH_{revp} in both Fig. 1a and b. Thereby, we have the possibility to model the ΔH curve thanks to its visibly monotonous variation.

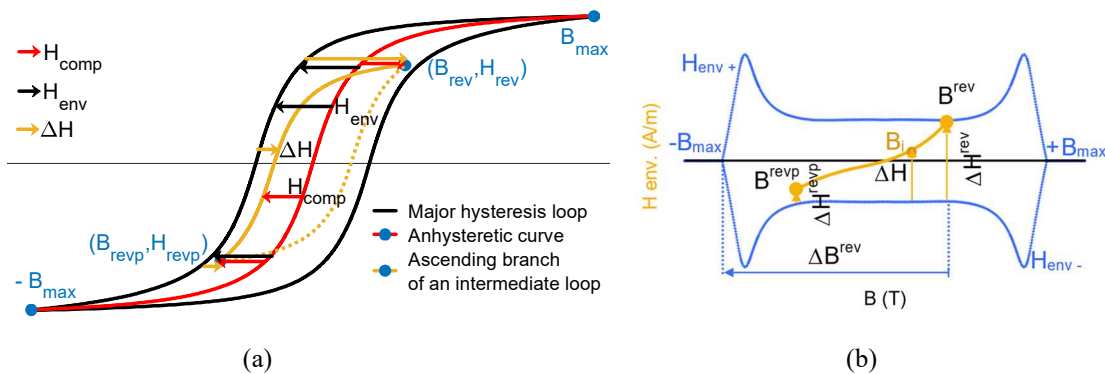


Fig. 1 (a) Demonstration of main notions based on the major and an intermediate hysteresis loop; (b) H_{env} and H_{comp} after eliminating H_{anhys}

2.1 Unit differential reversal curve (uDRC) – a model basis

In Fig. 2, more illustrative demonstration of ΔH is presented, where the field difference between many intermediate hysteresis loops and the major loop is represented in absolute $\Delta H(A/m)$ (Fig. 2a) and relative $\delta h(p.u)$ (Fig. 2b) scales. The plotted data is referred to the thin-gauge non-oriented SiFe NO20 (thickness of 0.2 mm). In the absolute scale, ΔH_{revp} is brought to zero, and hence the ΔH value of each curve is subtracted by the corresponding ΔH_{revp} value. In the relative scale, δh and δb are calculated as follows.

$$\delta h = \frac{\Delta H - \Delta H_{revp}}{\Delta H_{rev} - \Delta H_{revp}} ; \delta b = \frac{B - B_{revp}}{B_{rev} - B_{revp}} \quad (4)$$

As can be seen in Fig. 2, there is visibly a rule of change, particularly in Fig. 2b. As the induction amplitude of the hysteresis loop increases, δh curve varies more quickly at the beginning and rapidly approaches its minimum value. If we compare the relative δh of different curves at the same level of the relative δb , the higher the induction amplitude, the less the δh we have.

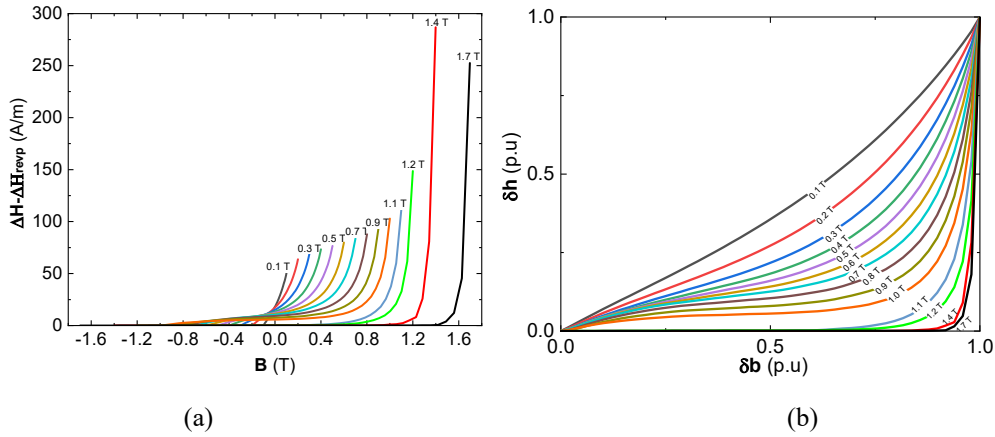


Fig. 2 (a) Absolute ΔH as a function of the induction of hysteresis loops at different level of induction amplitude (NO20 sample); (b) Normalized δh as a function of normalized δb of the same loops.

The progressive cancelation of δh is not only observed in the case of centered hysteresis loops but also in the case of reversal curves of any order (minor loops) as illustrated in Fig. 3. In the figure, three reversal curves of a hysteresis loop composing minor loops are analyzed. These curves have different value of B_{rev} , B_{revp} but their ΔH and δh curves all have the same kind of variation.

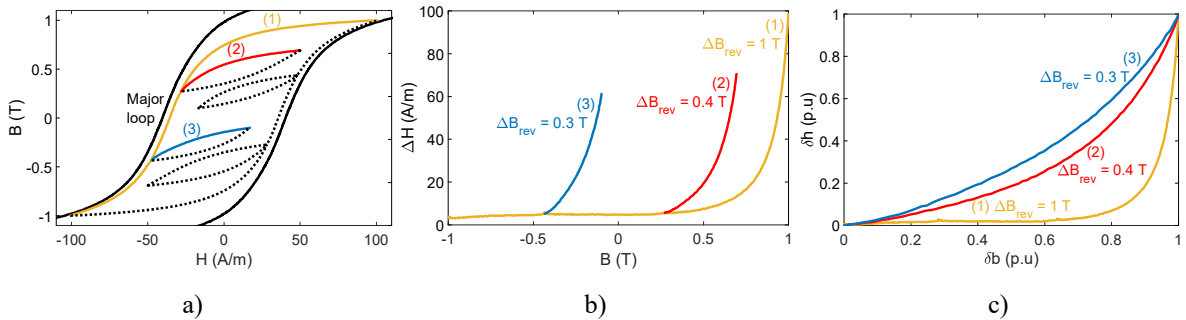


Fig. 3 Tested material: NO20; a) The major loop with $B_{max} = 1.75 T$ and a hysteresis loop composing minor loops; b) ΔH of three reversal curves; c) δh (uDRC) of three reversal curves

For this reason, by developing a model of the relative field difference δh , now called the unit differential reversal curve (uDRC), we can identify H_{comp} of any reversal curves through the following relationship.

$$H_{comp} = \Delta H + H_{env} = (\Delta H_{rev} - \Delta H_{revp}) \cdot \delta h + H_{env} ; \text{ where } \delta h = f(\Delta B_{rev}, \delta b) \quad (5)$$

with $(B_{rev}, \Delta H_{rev})$ and $(B_{revp}, \Delta H_{revp})$ are respectively the flux density and the field difference ΔH at the initial and the final magnetization states of a reversal curve. In the case of a centered hysteresis loop, $\Delta B_{rev} = (B_{rev} - B_{revp})/2$ representing the flux density amplitude.

2.3 uDRC model

In Equation (5), $f(\Delta B_{rev}, \delta b)$ can be any arbitrary function that increases monotonically following the increase of δb and fits experimental curves. Function coefficients are identified by applying curve fitting techniques to a set of input reversal curves. To ensure the simplicity of the model, we assume that centered hysteresis loops (zero-order and no-offset reversal curves) are sufficiently good approximations for higher-order reversal curves in the identification procedure. It implies that the function coefficients are identified based on centered minor loops that have ΔB_{rev} equal to the peak value of B and have no offset ($B_{rev} + B_{revp} = 0$). These coefficients are assumed applicable to the case of other reversal curves of any order, with or without offset.

We start to model each **uDRC** separately, then correlate model coefficients with ΔB_{rev} . It is natural to try firstly an exponential type function for such variation in Fig. 2b. A unit exponential function is chosen as follows, the variation speed of δh is adjusted by coefficient k_1 . The higher the ΔB_{rev} , the bigger k_1 we need.

$$f_1(\delta b) = \frac{e^{-k_1}}{1 - e^{-k_1}} (e^{k_1 \delta b} - 1) \text{ with } k_1 > 0, f(0) = 0 \text{ and } f(1) = 1 \quad (6)$$

A simple curve fitting technique allows us to identify k_1 . The obtained results show that there is an underestimation at the low level of δb , and an overestimation at the other level. An example can be found in Fig. 4, where the simulated curve resulted from f_1 (blue curve) does not match the measured curve (black dotted curve). To overcome this problem, we apply a weighted multiplier $f_2(\delta b)$. This multiplier must have considerably big value at low δb and low value at high δb . It must have a unit value (one) at $\delta b = 1$ to ensure that the final function varies between zero and one. f_2 is chosen as follow.

$$f_2(\delta b) = 1 + k_2 e^{-k_3} (e^{-k_3(\delta b - 1)} - 1) \text{ with } k_2, k_3 > 0, \text{ and } f_2(1) = 1 \quad (7)$$

And so on,

$$f(\delta b) = f_1 \cdot f_2 = [1 + k_2 e^{-k_3} (e^{-k_3(\delta b - 1)} - 1)] \cdot \frac{e^{-k_1}}{1 - e^{-k_1}} (e^{k_1 \delta b} - 1) \quad (8)$$

with $k_1(\Delta B_{rev}), k_2(\Delta B_{rev}), k_3(\Delta B_{rev}) > 0, f(0) = 0, \text{ and } f(1) = 1$

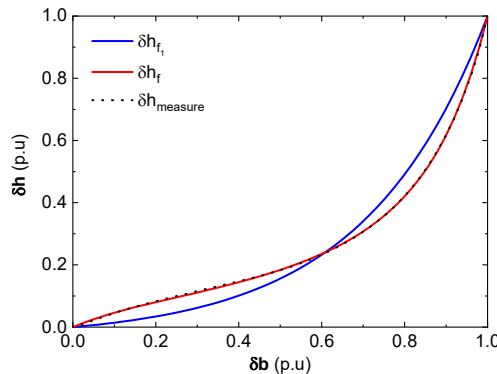


Fig. 4 Measured curve and two simulated curves of uDRC at 0.8 T (NO20 sample).

With the addition of f_2 , the resulted function fits the experimental data far better than before (the red curve in Fig. 4). Before proceeding to the last choice of f_2 , we have tested different functions and also various approaches. However, the above was finally chosen because its parameters k_2 and k_3 experimentally increase monotonously following ΔB_{rev} . This is a necessary condition to reduce the sensitivity and so on to increase the robustness of parameter identification procedure. As a consequence, we can greatly decrease the amount of input data while always maintaining the identification quality. A sensitivity analysis is presented in the next section.

Thereby, there is three parameters to identify for each δh curve. The normalized variation of parameters k_1, k_2 and k_3 following ΔB_{rev} are illustrated in Fig. 5a. It appears that these parameters follow an exponential-type rule and thus we can fit them using the following expression. The variation of k_2 also follows the exponential rule, but at the last step where the induction changes from 1.6 to 1.7 T, k_2 increases very quickly (around 100 times), and the last point of the curve is distinct from the other points.

$$k_1 = \alpha_1 \cdot e^{\lambda_1 \Delta B_{rev}^{Y_1}}; k_2 = \alpha_2 \cdot e^{\lambda_2 \Delta B_{rev}^{Y_2}}; k_3 = \alpha_3 \cdot e^{\lambda_3 \Delta B_{rev}^{Y_3}} \quad (9)$$

with $\alpha_{1,2,3}, \gamma_{1,2,3}, \lambda_{1,2,3} > 0$

The main advantage of this function type is its adjustable growth rate, which changes dramatically in the case of $k_{1,2,3}$ as shown in Fig. 5a. Finally, for an entire system of **uDRC**, we must identify a set of nine parameters $\alpha_{1,2,3}$, $\gamma_{1,2,3}$ and $\lambda_{1,2,3}$. The global identification procedure of the above parameters is programmed in MATLAB. We employ the *fgoalattain* function to minimize the difference between the model and experimental data. Simulated results with high accuracy for a thin gauge SiFe sample NO20 are demonstrated in Fig. 5b.

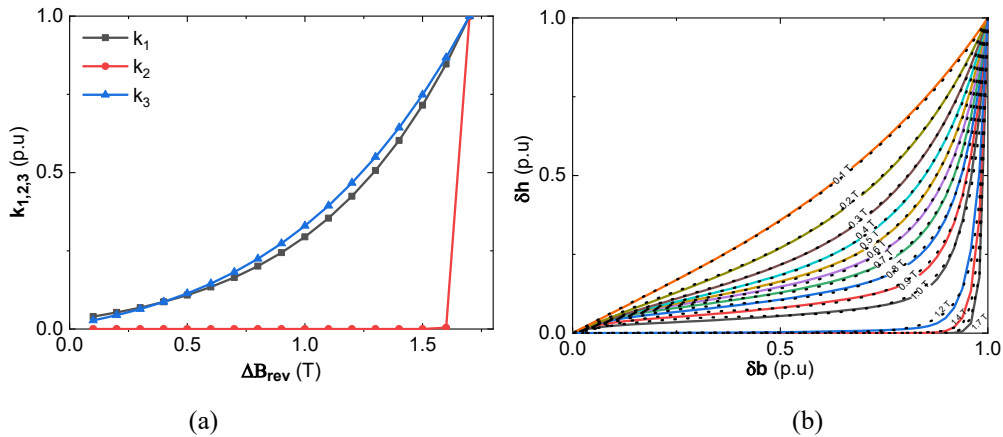


Fig. 5 (a) Variation of coefficients of f_2 as a function of ΔB_{rev} (NO20 sample); (b) Measured and simulated **uDRC** at different induction levels (NO20 sample).

2.3 General procedure of the model

For the reconstruction of a hysteresis loop, at any magnetization state of the material, we proceed the following steps to determine the magnetic field H_{stat} value.

- 1) Update the initial (B_{rev}, H_{rev}) and the final (B_{revp}, H_{revp}) reversal magnetization states using the history management strategy and then derive ΔB_{rev} , ΔH_{rev} and ΔH_{revp} ,
- 2) Interpolate the value of H_{anhys} and H_{env} at the actual magnetization state,
- 3) Normalize the induction value using Equation (4) and derive δh from the model of **uDRC**,
- 4) Derive H_{comp} using Equation (5), and finally update $H = H_{an} + H_{comp}$.

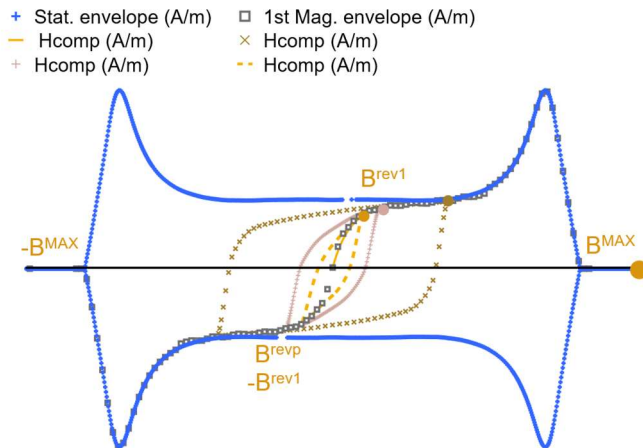


Fig. 6 H_{comp} reconstruction of three intermediate hysteresis loops with different amplitudes.

Fig. 6 illustrates examples of H_{comp} reconstruction. In this figure, we can observe all the base curves, namely the reduced anhysteretic curve (horizontal axis), two envelopes H_{env} (blue solid curves), and the first magnetization envelope (amber solid curve with unfilled square symbol). The latter is defined by the difference between the first magnetization curve (H_{1stM}) and the anhysteretic curve (H_{anhys}).

$$H_{1stMagEnv} = H_{1stMag} - H_{anhys} \quad (10)$$

The first magnetization envelope is important for the magnetic history management. Because, initially, we do not have any information of the previous magnetic state of the material, an initialization phase is thus necessary. It is convenient to consider that the starting state is always the fully demagnetized state ($H = 0, B = 0$). $B(H)$ path at the beginning follows the first magnetization curve. When the first reversal point (B_{rev1}, H_{rev1}) appears, $B(H)$

leaves the latter path and follows a new branch with $B_{revp1} = -B_{rev1}$. This approach ensures that a hysteresis loop whose input varies between equal positive and negative global extrema will have a symmetrical shape. It can be seen clearly in Fig. 6 the existence of the initial phase, the reversal points are attached to the first magnetization envelop $H_{1stMagEn}$ and two branches of H_{comp} of the three illustrated loops are always symmetrical.

2.4 Mechanism of memory formation

In the existing literature, the essence of hysteresis is constituted of history dependent branching. Back and forth variations between two consecutive extrema produce systematically descending and ascending branches of a hysteresis loop. Thereby, a hysteresis model has always a mechanism of memory formation, which detects local extrema, accumulates them, erases them and chooses the appropriate ones to produce the reversal hysteresis branches.

In our model, an extremum is detected progressively and numerically when there is a switch between back and forth variation, and vice versa. All the recognized extrema are stored into two stacks which follow the LIFO rule (last in, first out). A minimum stack stocks up with back-to-forth extrema and a maximum stack with forth-to-back extrema. Initially, both of stacks are empty, we initialize the reconstruction of hysteresis loop by following the first magnetization curve until an extremum (a reversal point) appears. After that, at each magnetization state, we update the stacks with one of the following operations.

- Accumulating: if an extremum is recognized as a minimum greater than the minima stored or a maximum smaller than the maxima stored, it is accumulated at the top of the related stack. In the case of the first recognized extremum B_{rev1} , its symmetrical point $B_{revp} = -B_{rev1}$ is also accumulated to ensure the symmetry of the major envelope.
- Erasing: if the input is raising and it is greater than one or several previously stored maxima at the same time, the latter maxima and also the same number of top minima must be wiped out. In contrast, if the input is decreasing and it is smaller than one or several previously stored minima at the same time, the latter minima and also the same number of top maxima must be wiped out. If the input is a new extremum, it must be accumulated at the top of the related stack. In general, only dominant input extrema are stored by the model.
- or nothing changes because the input keeps moving forward or backward, it is neither a new extremum, nor a violation of the erasing condition.

Next, the extremum on the top of both stacks is taken into account as B_{rev} and B_{revp} . If the reversal curve is an ascending branch (+), B_{rev} is a minimum and B_{revp} is a maximum. On the other hand, for a descending branch (-), B_{rev} is a maximum and B_{revp} is a minimum. The **uDRC** is then identified based on $\Delta B_{rev} = (B_{rev} - B_{revp})/2$. $\delta h, \Delta H$ and H_{comp} of the corresponding magnetization state are finally systematically derived. In contrast to the classical Preisach model, our model does not have the congruency property. Minor hysteresis loops corresponding to back-and-forth variations of inputs between the same two consecutive extremum values, having the same ΔB_{rev} , are not congruent even they certainly have the same **uDRC**. Because the **uDRC** is always scaled up with $(\Delta H_{rev} - \Delta H_{revp})$ which varies according to the accumulated magnetic memory.

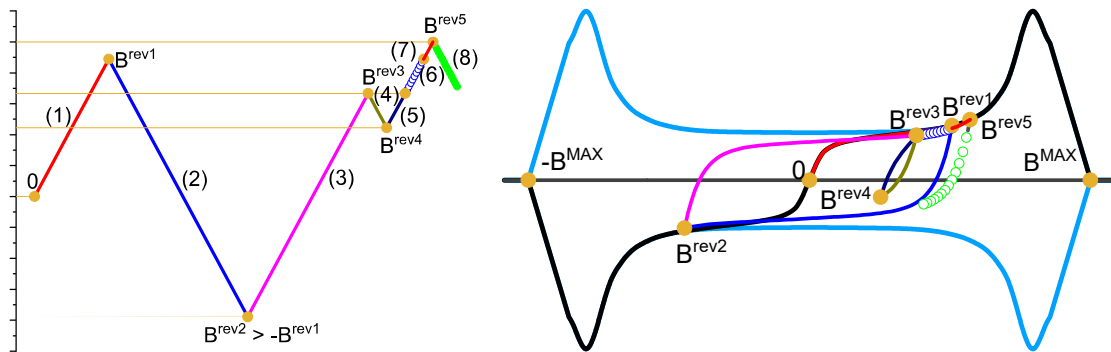


Fig. 7 Example of the mechanism of memory formation: (a) Variation of $B(t)$; (b) Variation of H_{comp} .

Fig. 7 and Table I represent an example of memory formation. The B-waveform is divided into 8 segments.

- Segment 1: initialization phase, H_{comp} follows the $H_{1stMagEn}$ curve till B_{re} ,

- Segment 2: B_{rev1} and $-B_{rev1}$ are respectively accumulated to the max and min stacks, a descending curve of H_{comp} is produced which passes through $(B_{rev1}, -B_{rev1})$,
- Segment 3: because $B_{rev} > -B_{rev1}$, it is accumulated to the min stack, an ascending curve of H_{comp} is produced which passes through (B_{rev2}, B_{rev1}) ,
- Segment 4: because $B_{rev} < B_{rev1}$, it is accumulated to the max stack, a descending curve of H_{comp} is produced which passes through (B_{rev3}, B_{rev2}) ,
- Segment 5: because $B_{rev4} > B_{rev2}$, it is accumulated to the min stack, an ascending curve of H_{comp} is produced which passes through (B_{rev4}, B_{rev3}) ,
- Segment 6: when the input induction B is greater than B_{rev3} , the program erases B_{rev3} of the max stack and B_{rev4} of the min stack, an ascending curve of H_{comp} is produced which passes through (B_{rev2}, B_{rev1}) ,
- Segment 7: when the input induction B is greater than B_{rev1} , the program erases B_{rev1} of the max stack, B_{rev2} and $-B_{rev}$ of the min stack, the $-B_{rev}$ is also erased to ensure the major envelope always has the same shape regardless the existence of minor loops. An ascending curve of H_{comp} is produced following the $H_{1stMagEnv}$ curve as in the initialization phase,
- Segment 8: a descending curve of H_{comp} is produced which passes through $(B_{rev5}, -B_{rev5})$.

Table 1 Minimum and maximum stacks at the beginning of each segment of the induction waveform presented in Fig. 7

Segment 1 (+)		Segment 2 (-)		Segment 3 (+)		Segment 4 (-)		Segment 5 (+)		Segment 6 (+)		Segment 7 (+)		Segment 8 (-)	
Min n/a	Max n/a	Min - B^{rev1}	Max B^{rev1}	Min B^{rev2}	Max B^{rev1}	Min B^{rev2}	Max B^{rev3}	Min B^{rev4}	Max B^{rev3}	Min B^{rev2}	Max B^{rev1}	Min n/a	Max n/a	Min B^{rev5}	Max - B^{rev5}
					- B^{rev1}		B^{rev1}	B^{rev2}	B^{rev1}	- B^{rev1}					

2.5 Model extrapolation

Beyond the limit of the experimental input data, hysteresis loops are constructed considering several hypotheses. The anhysteretic curve is firstly extrapolated by the expression of Frolich-Kennely [32] to extend the reversible range. Next, when the first magnetization curve and two hysteresis branches reach a level above the amplitude B_{max} of the major loop, they are assumed to be merged with the anhysteretic curve. Therefore, beyond this level, magnetic behavior is considered reversible. We can improve this deficiency by increasing B_{max} . Thanks to an advanced magnetic characterization system described in [33], B_{max} can attain 95% of the saturation polarization of any ferromagnetic materials. On the other hand, an extrapolation of envelop curves H_{env} can further enhance the accuracy of our model in this minor region. This improvement will shortly be realized.

An example of how the anhysteretic curve is extrapolated is presented in Fig. 8.

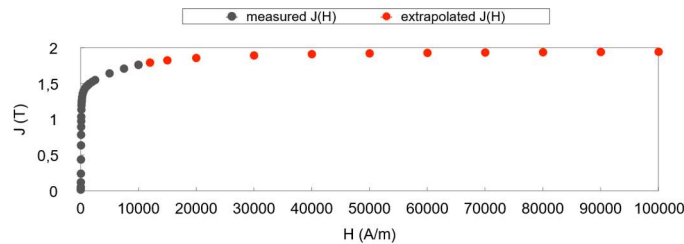


Fig. 8 Example of anhysteretic curve extrapolation.

3. RESULTS

3.1 Centered hysteresis loops

The model has been built in MATLAB comprising two distinct tools, one for the automatic identification of the model and the other for the construction of hysteresis loops and subsequent interpretation. The new LS static model has been applied for most of ferromagnetic material families, such as SiFe, CoFe, NiFe and amorphous alloys. Thereafter, the performance of this model will be verified through a series of measurement performed with a thin-gauge (0.2 mm) non-oriented SiFe alloy, NO20, which is currently used extensively in various low-loss applications.

For the identification of the model, quasi-static measurements have been realized under the following conditions:

- Frequency: 5 Hz,

- Induction waveform: controlled-triangular waveform,
- Induction amplitude of the major loop: 1.75 T (corresponding to a magnetic field of 11 000 A/m),
- Induction amplitude of intermediate loops: 0.1 T to 1.7 T with a step of 0.1 T, 17 loops in total.

It is worth noting that the saturation polarization of NO20 is approximately 1.9 T. Three entry sets, detailed below, with different amounts of data are assigned to identify the model, allowing to analyze the model sensitivity to input.

- SET1 comprises the whole 17 measured loops,
- SET2 with 9 loops having the following amplitudes $\{0.1, 0.3, 0.5, 0.7, 0.9, 1.1, 1.3, 1.5, 1.7\}$ T,
- SET3 with 5 loops having the following amplitudes $\{0.1, 0.5, 0.9, 1.3, 1.7\}$ T.

The resulted parameters α, γ, λ are presented in Table II. The relative iron loss **deviation** of each hysteresis loop in comparison with the experiment ($\frac{Loss_{simulation} - Loss_{measure}}{Loss_{measure}} * 100\%$) is also calculated and detailed in Table III. As can be seen, the variation of the model parameters and relative iron loss **deviation** of each data set are very small, confirming that the function $f(\Delta B_{rev}, \delta b)$ is a consistent representation of **uDRC**. In addition, after each execution of the identification procedure, the obtained combination of coefficients is unique. The predictive capacity of the model is partly demonstrated by exact centered hysteresis loops, especially those that are not part of **SET2** and **SET3**. In Fig. 9a, a comparison between simulated and measured loops at 0.8 T is presented, with loops identified based on **SET2** and **SET3** shifted deliberately to the left and the right respectively to increase the visibility of the comparison. Without this treatment, all simulated and measured loops coincide for the most part. In Fig. 9b, several simulated and measured symmetrical loops are introduced.

Table II Model parameters identified with three input data sets (values are presented in p.u system where the coefficients of the SET1 are defined as the base unit)

	α_1 (p.u)	γ_1 (p.u)	λ_1 (p.u)	α_2 (p.u)	γ_2 (p.u)	λ_2 (p.u)	α_3 (p.u)	γ_3 (p.u)	λ_3 (p.u)
SET1	1.00	1.00	1.00	1.00	1.00	1.00	1.00	1.00	1.00
SET2	1.05	1.03	0.96	1.07	1.00	0.94	1.39	1.12	0.90
SET3	1.04	1.06	0.96	1.00	1.04	0.95	1.19	1.08	0.94

Table III Relative iron loss **deviation** of all intermediate cycles calculated by models identified by three sets of data

Amplitude (T)	0.1	0.2	0.3	0.4	0.5	0.6	0.7	0.8	0.9	1.0	1.1	1.2	1.3	1.4	1.5	1.6	1.7
SET1 (%)	-0.1	-0.1	-0.1	-0.1	-0.1	-0.1	-0.7	-0.6	-0.1	-0.1	-0.1	-0.1	-2.5	-1.5	-0.1	-1.0	-2.1
SET2 (%)	0.9	0.6	-0.1	-0.3	-0.4	-0.3	-0.7	-0.3	0.5	0.5	0.3	-0.1	-2.9	-2.0	-0.5	-1.3	-2.4
SET3 (%)	0.8	-0.1	0.1	0.7	0.9	0.5	-1.2	2.5	3.0	-2.9	-2.0	-1.2	-3.2	-1.9	-0.3	-1.1	-2.1

In addition to the result of the NO20 sample, we also summary some notable results obtained with other materials, namely CoFe, NiFe and classical SiFe M800-50A. In Table IV, the new LS static model of each material is identified using three sets of data (two in the case of M800-50A). The number of loops in each set is respectively 20, 10, 7 for the CoFe sample, 16, 8, 6 for the NiFe sample and 10, 5 for the M800-50A sample. For each sample, all the loops of SET1 are reconstructed using the three models. The comparison procedure as in the case of the NO20 sample is reproduced. In the Table IV, we present the average relative iron loss **deviation** of all loops (sum of all **deviation** values divided by the number of loops) and also the relative iron loss **deviation** of the worst simulated hysteresis loop.

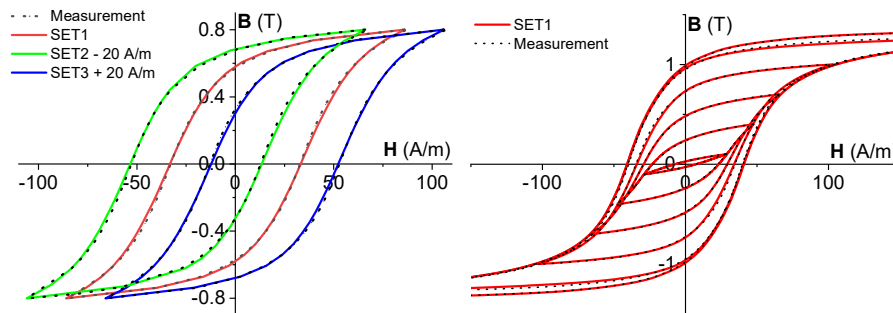


Fig. 9 (a) Hysteresis loops resulted from three sets of data (NO20 sample); (b) Comparison between simulation and experiment in the case of several intermediate loops (NO20 samples).

The average **deviation** of all data sets is consistently low, which means that most loops are reconstructed with high accuracy. Besides, the worst result achieved so far is a **deviation** of 5.1%, which is highly acceptable. Therefore, we can conclude that SET3 (five to seven input hysteresis loops) have already enough input data for identifying coefficients of the model of any lamination. The presented fitting function is shown to be sufficiently robust to represent **uDRC** curves with a small amount of input data. Regarding the model identification, to have a same accuracy, the being studied model requires much less data than the Preisach model.

Table IV Notable results found for different materials

Material	J_s (T)	B_{max} (T)	The average relative deviation (%)			The worst relative deviation (%)		
			SET1 (%)	SET2 (%)	SET3 (%)	SET1 (%)	SET2 (%)	SET3 (%)
NO20	1.9	1.75	0.6	0.8	1.4	2.5	2.9	3.2
CoFe	2.4	2.1	0.5	0.6	0.7	1.1	1.6	1.9
NiFe	1.6	1.55	0.6	0.7	1.5	3.3	3.1	4.9
M800-50A	2.0	1.8	~	1.0	1.1	~	2.6	5.1

3.2 Hysteresis loops containing minor loops

The prediction capability of the model is validated using hysteresis loops containing minor loops. These loops are measured by imposing an induction waveform that includes harmonics up to rank 11. Each element of this validation set is abbreviated as $HX - Y - Z$. This means that the induction signal $B(t)$ is a sinusoidal signal comprising a harmonic of rank X , having an amplitude $Y\%$ of the fundamental and a phase shift of Z degree. For example, the signal designated by H3-50-60 corresponds to a fundamental to which we add 50% of a 60°-shifted 3rd harmonic. Results of a combination of four induction waveforms and three levels of amplitude are reported in Table V. It is apparent that iron loss prediction is consistently good, and the worst discrepancy is -5.0% which is highly acceptable. This underestimated **deviation** may be explained by the dynamic effect of the material. Although the fundamental frequency is 5 Hz, its 11th order harmonics is already 55 Hz which significantly increases the importance of the dynamic effect. In Fig. 11, three simulated loops are compared with their experimental loops. As can be seen, despite over- and underestimation, the **deviation** is insignificant and reversal curves are well-represented. Another notable result is presented in Fig. 11d, where the simulated demagnetization hysteresis curve coincides with the experiment in most part. The induction waveform in this case is imposed to have an initial amplitude of 1.7 T, which reduces progressively to the demagnetized state after 17 back and forth variations (Fig. 10).

Table V Relative iron losses in the case of harmonic-added signals for the NO20 sample

Signal type	H3-50-60			H5-50-60			H5-25-180			H11-25-60		
Amplitude (T)	0.5	1	1.5	0.5	1	1.5	0.5	1	1.5	0.5	1	1.5
SET1 (%)	0.5	2.0	3.8	-2.0	-0.2	-0.1	-2.2	-0.6	3.2	-3.9	-2.1	-4.6
SET2 (%)	0.1	2.5	3.4	-2.2	0.2	-0.4	-2.6	-0.1	2.8	-4.2	-1.7	-5.0
SET3 (%)	1.3	-0.7	3.5	-1.2	-2.7	-0.4	-1.4	-3.4	3.0	-3.2	-4.7	-5.0

4. CONCLUSIONS

A new static LS model has been developed and presented in this paper. Its principle has been described in detail, following by the complete validation procedure. All these steps proved the simplicity of both the idea and the implementation, as well as the accuracy of the model. The model is expected to be extremely useful for the representation of the material static behavior whatever the magnetization conditions based on very few experimental data (the experimental first magnetization curve and five to seven intermediate hysteresis loops). Currently, this new version is being implemented in the Altair FLUX FEM simulation software to replace the older version, which is less accurate. With the upcoming release of an improved version of the dynamic part, the Loss Surface model promises to represent the behavior of ferromagnetic materials in a very reliable way.

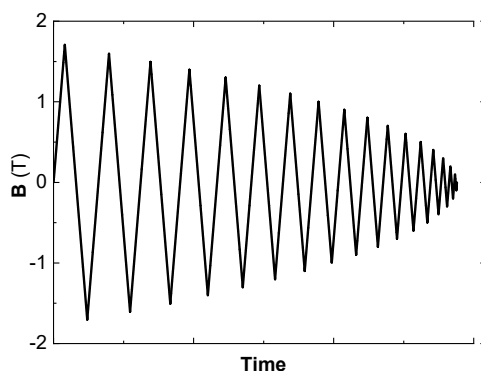


Fig. 10 Induction waveform of a demagnetization hysteresis loop with a wavelength of 1 second.

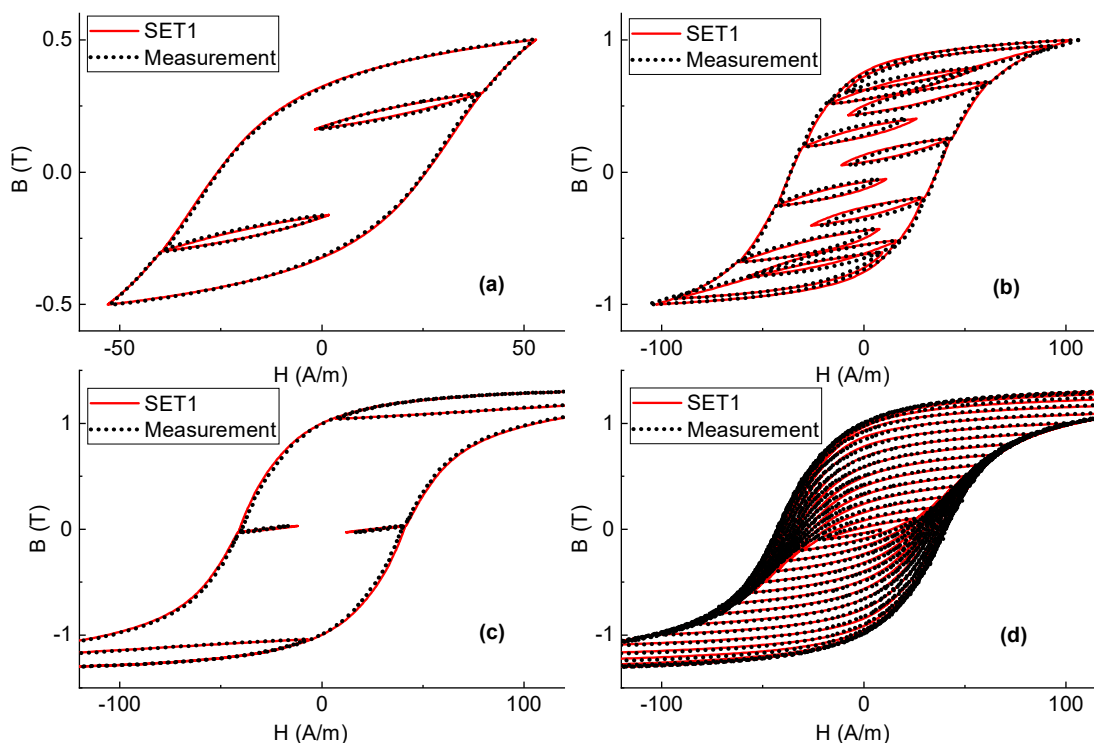


Fig. 11 Comparison between simulation and experiment (NO20 sample): (a) H3-50-60, 0.5 T; (b) H11-25-60, 1.0 T; (c) H5-60-180, 1.5 T; (d) demagnetization signal.

REFERENCES

- [1] A. T. D. Almeida, F. J. T. E. T. E. Ferreira, et J. A. C. Fong, « Standards for Efficiency of Electric Motors », IEEE Ind. Appl. Mag., vol. 17, no 1, p. 12-19, janv. 2011.
- [2] C. P. Steinmetz, « On the law of hysteresis », Proc. IEEE, vol. 72, no 2, p. 197-221, févr. 1984.
- [3] R. H. Pry et C. P. Bean, « Calculation of the Energy Loss in Magnetic Sheet Materials Using a Domain Model », J. Appl. Phys., vol. 29, no 3, p. 532-533, mars 1958.
- [4] G. Bertotti, « General properties of power losses in soft ferromagnetic materials », IEEE Trans. Magn., vol. 24, no 1, p. 621-630, janv. 1988.
- [5] M. Amar et R. Kaczmarek, « A general formula for prediction of iron losses under nonsinusoidal voltage waveform », IEEE Trans. Magn., vol. 31, no 5, p. 2504-2509, sept. 1995.
- [6] A. Boglietti, A. Cavagnino, D. M. Ionel, M. Popescu, D. A. Staton, et S. Vaschetto, « A General Model to Predict the Iron Losses in PWM Inverter-Fed Induction Motors », IEEE Trans. Ind. Appl., vol. 46, no 5, p. 1882-1890, sept. 2010.
- [7] M. Popescu, D. M. Ionel, A. Boglietti, A. Cavagnino, C. Cossar, et M. I. McGilp, « A General Model for Estimating the Laminated Steel Losses Under PWM Voltage Supply », IEEE Trans. Ind. Appl., vol. 46, no 4, p. 1389-1396, juill. 2010.
- [8] Jieli Li, T. Abdallah, et C. R. Sullivan, « Improved calculation of core loss with nonsinusoidal waveforms », in Conference Record of the 2001 IEEE Industry Applications Conference. 36th IAS Annual Meeting (Cat. No.01CH37248), 2001, vol. 4, p. 2203-2210 vol.4.
- [9] K. Venkatachalam, C. R. Sullivan, T. Abdallah, et H. Tacca, « Accurate prediction of ferrite core loss with nonsinusoidal waveforms using only Steinmetz parameters », in 2002 IEEE Workshop on Computers in Power Electronics, 2002. Proceedings., 2002, p. 36-41.
- [10] D. M. Ionel, M. Popescu, S. J. Dellinger, T. J. E. Miller, R. J. Heideman, et M. I. McGilp, « On the variation with flux and frequency of the core loss coefficients in electrical machines », IEEE Trans. Ind. Appl., vol. 42, no 3, p. 658-667, mai 2006.
- [11] D. M. Ionel, M. Popescu, M. I. McGilp, T. J. E. Miller, S. J. Dellinger, et R. J. Heideman, « Computation of Core Losses in Electrical Machines Using Improved Models for Laminated Steel », IEEE Trans. Ind. Appl., vol. 43, no 6, p. 1554-1564, nov. 2007.

- [12] A. T. Vo, M. Fassenet, L. Arbenz, A. Kedous-Lebouc, et C. Espanet, « An analysis of power losses in nanocrystalline and thin-gauge non-oriented SiFe materials for application to high-speed electrical machines », *The European Physical Journal Applied Physics (EPJ AP)*, 2019.
- [13] A. Krings et J. Soulard, « Overview and comparison of iron loss models for electrical machines », *J. Electr. Eng.*, vol. 10, no 3, p. 162-169, 2010.
- [14] F. Preisach, « Über die magnetische Nachwirkung », *Z. Für Phys.*, vol. 94, no 5, p. 277-302, mai 1935.
- [15] I. D. Mayergoyz, *Mathematical models of hysteresis and their applications*. Academic Press, 2003.
- [16] D. C. Jiles et D. L. Atherton, « Theory of ferromagnetic hysteresis », *J. Magn. Magn. Mater.*, vol. 61, no 1-2, p. 48-60, 1986.
- [17] A. Bergqvist, « Magnetic vector hysteresis model with dry friction-like pinning », *Phys. B Condens. Matter*, vol. 233, no 4, p. 342-347, 1997.
- [18] F. Henrotte, A. Nicolet, et K. Hameyer, « An energy-based vector hysteresis model for ferromagnetic materials », *COMPEL- Int. J. Comput. Math. Electr. Electron. Eng.*, vol. 25, no 1, p. 71-80, 2006.
- [19] S. Bobbio, G. Milano, C. Serpico, et C. Visone, « Models of magnetic hysteresis based on play and stop hysterons », *IEEE Trans. Magn.*, vol. 33, no 6, p. 4417-4426, nov. 1997.
- [20] S. E. Zirka, Y. I. Moroz, P. Marketos, et A. J. Moses, « Viscosity-based magnetodynamic model of soft magnetic materials », *IEEE Trans. Magn.*, vol. 42, no 9, p. 2121-2132, sept. 2006.
- [21] R. G. Harrison, « Physical Theory of Ferromagnetic First-Order Return Curves », *IEEE Trans. Magn.*, vol. 45, no 4, p. 1922-1939, avr. 2009.
- [22] R. G. Harrison, « Modeling High-Order Ferromagnetic Hysteretic Minor Loops and Spirals Using a Generalized Positive-Feedback Theory », *IEEE Trans. Magn.*, vol. 48, no 3, p. 1115-1129, mars 2012.
- [23] K. Jacques, R. V. Sabariego, C. Geuzaine, et J. Gyselinck, « Inclusion of a Direct and Inverse Energy-Consistent Hysteresis Model in Dual Magnetostatic Finite-Element Formulations », *IEEE Trans. Magn.*, vol. 52, no 3, p. 1-4, 2015.
- [24] K. Jacques, S. Steentjes, F. Henrotte, C. Geuzaine, et K. Hameyer, « Representation of microstructural features and magnetic anisotropy of electrical steels in an energy-based vector hysteresis model », *AIP Adv.*, vol. 8, no 4, p. 047602, 2018.
- [25] T. Chevalier, A. Kedous-Labouc, B. Cornut, et C. Cester, « Estimation of magnetic loss in an induction motor fed with sinusoidal supply using a finite element software and a new approach to dynamic hysteresis », *IEEE Trans. Magn.*, vol. 35, no 5, p. 3400-3402, sept. 1999.
- [26] T. Chevalier, A. Kedous-Lebouc, B. Cornut, et C. Cester, « A new dynamic hysteresis model for electrical steel sheet », *Phys. B Condens. Matter*, vol. 275, no 1, p. 197-201, janv. 2000.
- [27] L. Li, A. Kedous-Lebouc, A. Foggia, et J. Mipo, « Influence of Magnetic Materials on Claw Pole Machines Behavior », *IEEE Trans. Magn.*, vol. 46, no 2, p. 574-577, févr. 2010.
- [28] A. Frias, A. Kedous-Lebouc, C. Chillet, L. Albert, et L. Calegari, « Improvement and validation of an iron loss model for synchronous machine », in *2012 XXth International Conference on Electrical Machines*, 2012, p. 1328-1332.
- [29] A. Frias, « Minimisation des pertes fer des machines électriques de traction par la modélisation et l'optimisation », PhD dissertation, Grenoble Alpes, 2015.
- [30] S. E. Zirka, Y. I. Moroz, R. G. Harrison, et K. Chwastek, « On physical aspects of the Jiles-Atherton hysteresis models », *J. Appl. Phys.*, vol. 112, no 4, p. 043916, août 2012.
- [31] J. Pearson, P. T. Squire, et D. Atkinson, « Which anhysteretic magnetization curve? », *IEEE Trans. Magn.*, vol. 33, no 5, p. 3970-3972, sept. 1997.
- [32] S. L. Gokhale, « Law of magnetization », *Trans. Am. Inst. Electr. Eng.*, vol. 45, p. 1013-1035, 1926.
- [33] A. Vo, M. Fassenet, A. Lebouc, F. Blache, C. Boudinet and M. Vaillant, "Novel Adaptive Controller for Effective Magnetic Measurement Under Arbitrary Magnetization," in *IEEE Transactions on Industrial Electronics*. doi: 10.1109/TIE.2019.2955422